# The Intraflagellar Transport Protein Ift80 Is Essential for Photoreceptor Survival in a Zebrafish Model of Jeune Asphyxiating Thoracic Dystrophy

*Leah M. Hudak, Shannon Lunt, Chi-Hsuan Chang, Ethan Winkler, Halley Flammer, Michael Lindsey, and Brian D. Perkins*

**Purpose.** Jeune's asphyxiating thoracic dystrophy (JATD) is an autosomal recessive disorder with symptoms of retinal degeneration, kidney cysts, and chondrodysplasia and results from mutations in the *ift80* gene. This study was conducted to characterize zebrafish lacking *ift80* function for photoreceptor degeneration and defects in ciliogenesis to establish zebrafish as a vertebrate model for visual dysfunction in JATD and to determine whether *ift80* interacts genetically with Bardet-Biedl syndrome (BBS) genes.

**Methods.** Zebrafish were injected with morpholinos (MOs) targeted to the *ift80* gene. Retinas were analyzed by histology, transmission electron microscopy, and immunohistochemistry. Ear and kidney cilia were analyzed by whole-mount immunostaining. Intraflagellar transport (IFT) particle composition was subjected to Western blot analysis. Genetic interactions were tested by coinjection of MOs against *ift80* and *bbs4* or *bbs8* followed by in situ hybridization.

**Results.** Zebrafish lacking *ift80* function exhibited defects in photoreceptor outer segment formation and photoreceptor death. Staining with opsin antibodies revealed opsin mislocalization in both rods and cones. Ultrastructural analysis showed abnormal disc stacking and shortened photoreceptor outer segments. The kinocilia of the ear and motile cilia in the kidney were shorter and reduced in number. Western blot analysis revealed a slight increase in the stability of other IFT proteins. Coinjection of MOs against *ift80* and BBS genes led to convergent-extension defects.

**Conclusions.** Zebrafish lacking *ift80* exhibited defects characteristic of JATD. Because the developing outer segments degenerated, Ift80 could possibly act as a maintenance factor for the IFT particle. (*Invest Ophthalmol Vis Sci.* 2010;51: 3792–3799) DOI:10.1167/iovs.09-4312

Cilia are microtubule-based structures that protrude from almost all eukaryotic cells, including photoreceptors.[1] As sensory antennae,[2] vertebrate photoreceptors rely on a modified sensory cilia (i.e., the outer segment) for function. Mutations affecting cilia biogenesis or function cause pleiotropic symptoms frequently observed in a spectrum of hereditary diseases known as ciliopathies.[3] Such diseases include Bardet-Biedl syndrome (BBS), Senior-Løken syndrome, Meckel-Gruber syndrome, and Jeune asphyxiating thoracic dystrophy (JATD). Defects in the motile cilia that generate fluid flow within the respiratory epithelia and move cerebrospinal fluid result in fluid accumulation within the lungs, brain, and spine. Situs inversus stems from loss of cilia, which help establish left-right asymmetry, in the embryonic node. In the nonmotile sensory cilia, receptor molecules and ion channels decorate the ciliary membrane to detect signaling ligands and changes to the extracellular environment. Thus, ciliopathies often manifest with retinal degeneration, situs inversus, sensorineural hearing loss, mental impairment, and disorders of the kidney, liver, and pancreas.[4]

Cilia biogenesis requires intraflagellar transport (IFT) to build and maintain the microtubule axoneme.[5] IFT refers to the bidirectional movement of IFT particles along the axoneme. IFT particles are composed of at least 17 distinct IFT proteins. The molecular motors kinesin-II and cytoplasmic dynein 2 control anterograde and retrograde movement, respectively. IFT transports proteins necessary for cilia assembly and for specific cargos, such as membrane-bound receptors or ion channels. In photoreceptors, IFT is essential for outer segment formation and maintenance.[6–8]

JATD, also known as Jeune syndrome, is a rare, multisystem, autosomal recessive disorder that often results in neonatal lethality.[9,10] Mutations in the gene for *IFT80*, a component of the IFT particle, were recently found in a subset of patients with JATD.[11] JATD is principally characterized by abnormal skeletal development resulting in a long, narrow thorax, short ribs, shortened long bones, and occasional polydactyly.[12] Of the 20% of patients who survive beyond the neonatal period, many develop kidney cysts, hepatic fibrosis, and pancreatic abnormalities.[13] In milder cases, patients also exhibit reduced scotopic and photopic ERG amplitudes and night blindness as early as 5 years of age.[14–18] Postmortem pathology findings of an 8-year-old JATD patient revealed rod and cone degeneration and gliosis in the inner retina.[17] Because JATD shares features with other ciliopathies,[4] it would be useful to examine the loss-of-function phenotype in a genetically tractable model organism to understand the basis of retinal degeneration and to examine other ciliated cell types for dysfunction. Furthermore, genes associated with ciliopathies show epistatic effects with each other,[19,20] and some alleles can act as modifiers toward pathogenesis in ciliopathies.[21] Thus, exploring genetic interactions between *IFT80* and other disease-causing loci may provide insight into the molecular basis of JATD and identify other loci that contribute to JATD symptoms.

Null mutations in mouse IFT genes cause embryonic lethality between embryonic day (E)10.5 and E13.5, thus preventing examination of cell types such as photoreceptors that differentiate near birth or during postnatal periods.[22–25] In contrast,

From the Department of Biology, Texas A&M University, College Station, Texas.

Supported by National Institutes of Health Grant EY017037 (BDP).

Submitted for publication July 14, 2009; revised January 7 and February 6, 2010; accepted February 11, 2010.

Disclosure: **L.M. Hudak**, None; **S. Lunt**, None; **C.-H. Chang**, None; **E. Winkler**, None; **H. Flammer**, None; **M. Lindsey**, None; **B.D. Perkins**, None

Corresponding author: Brian D. Perkins, Department of Biology, Texas A&M University, 3258 TAMU, College Station, TX 77843; bperkins@mail.bio.tamu.edu.

zebrafish develop rapidly, with photoreceptor differentiation starting at 50 to 52 hours postfertilization (hpf); robust visual behaviors are present by 5 days postfertilization (dpf).[26,27] Although zebrafish IFT mutants die at 8 to 9 dpf, the effects of these mutations on photoreceptor structure and function can be investigated. We report that zebrafish deficient for *ift80* function exhibit phenotypes consistent with those of previously described IFT mutants and with symptoms associated with JATD. Morpholino knockdown of *ift80* disrupted photoreceptor outer segment structure and caused opsin mislocalization. In embryos lacking *ift80* function, cilia were disrupted in the kidney and otic vesicle. Finally, we show that *ift80* genetically interacts with *bbs4* and *bbs8* to regulate cell movement during gastrulation. Our results show that loss of *ift80* results in photoreceptor degeneration and that zebrafish may serve as a useful model for retinal dysfunction in JATD.

## Materials and Methods

### Fish Maintenance and Breeding

Wild-type zebrafish of the AB strain were housed, bred, and staged according to standard procedures.[28] Zebrafish were treated in accordance with the ARVO Statement for the Use of Animals in Ophthalmic and Vision Research.

### Morpholino Knockdown

*ift80* knockdown was carried out using a morpholino targeted to the splice site at the 3′ end of the second exon. Morpholinos were injected into wild-type embryos at the 1- to 2-cell stage according to standard procedures.[29] Morpholino sequences were as follows: *ift80*, AGGTGTATGTGGAACCTGTGATAAG; *bbs4*, GAAAAAGATCACTACTGTAAAGCAT; *bbs8*, AGCTGTATACTCACGAGCCACCTGA. The *ift80* morpholino was described previously,[11] and the *bbs4* and *bbs8* morpholinos were described by Gerdes et al.[30] and Yen et al.,[31] respectively.

### Transmission Electron Microscopy

Animals were fixed at 96 hpf in 1% paraformaldehyde, 2.5% glutaraldehyde, and 1% tannic acid. Embryos were processed with osmium tetroxide as secondary fixative, followed by a dehydration series in ethanol, and were infiltrated with epoxy resin as previously described.[32] Transverse sections (0.1 $\mu$m in thickness) obtained at the optic nerve region were poststained with 2% uranyl acetate and Reynolds lead citrate. Images were collected on a transmission electron microscope (1200EX; JEOL 1200EX, Tokyo, Japan) and were processed with image editing software (Photoshop; Adobe, Mountain View, CA).

### In Situ Hybridization and Reverse Transcription–Polymerase Chain Reaction

Digoxigenin-labeled (DIG) antisense riboprobes were synthesized from partial or full-length cDNAs using standard protocols. The *pax2.1* and *myoD* full-length cDNAs were gifts from Arne Lekven. In situ hybridizations were performed as previously described.[33] RT-PCR was performed using standard protocols.

### Image Analysis of Whole-Mount and Flat-Mount Embryos

Whole-mounted embryos were imaged with a stereomicroscope (Lumar; Carl Zeiss, Jena, Germany) and photographed with a digital camera (AxioCam; Carl Zeiss). Embryos were prepared for flat-mounting by dissecting the yolk away from the embryo proper with a small needle and were mounted in glycerol on glass slides. Commercial software (Axio Imager; Carl Zeiss) was used to measure embryo lengths from the anterior-most region of *pax2a* staining to the tip of the paraxial mesoderm *myoD* staining. Statistical analysis with appropriate software (Excel; Microsoft, Redmond, WA).

### Immunohistochemistry

Immunohistochemistry was performed as previously described.[34] Images were obtained on a fluorescence microscope (ImagerZ1; Carl Zeiss) fitted with a fluorescence microscope slider module (ApoTome; Carl Zeiss) using a 63× oil objective. Images were prepared using image editing software (Photoshop; Adobe). The monoclonal antibody 1D1 (Fadool JM, et al. *IOVS.* 1999;40:ARVO Abstract 1251) and the monoclonal antibody zpr-1 (Zebrafish International Resource Center) were both used at 1:200. Affinity-purified polyclonal rabbit antibodies against zebrafish IFT88 (1:5000) and zebrafish IFT52 (1:3000) were used as previously described.[32] Affinity-purified polyclonal rabbit antibodies against the blue cone opsin antibody (1:200), a gift from David Hyde, were used as previously described.[35] Affinity-purified polyclonal rabbit antibodies against mouse Centrin-3 were used at 1:200.[36] The appropriate fluorescently conjugated Alexa secondary antibodies (Invitrogen) were used at 1:500. Slides were counterstained with DAPI (Invitrogen, Carlsbad, CA) to label DNA.

### TUNEL Assays

Embryos were fixed at various time points and prepared for cryosectioning as described. TUNEL assays were performed on 10-$\mu$m–thick cryosections with an FITC label (In situ Cell Death Detection Kit; Roche Applied Sciences, Basel, Switzerland) according to the manufacturer's instructions. Images were obtained on a fluorescence microscope (ImagerZ1; Carl Zeiss) fitted with a fluorescence microscope slider module (ApoTome; Carl Zeiss) using a 20× objective. Five to 10 animals were imaged for each time point, and multiple distinct cryosections surrounding the optic nerve were analyzed for each retina. Between 26 and 81 data points were averaged for wild-type and *ift80* morphant embryos at each age and were compared using a two-tailed Student's *t*-test with unequal variance.

### SDS-PAGE and Immunoblot Analysis

Western blot analysis was performed as previously described.[32] The following dilutions of primary antibodies were used: monoclonal K2.4 (KIF3A, 1:10,000; Covance, Madison, WI); affinity-purified polyclonal rabbit antibodies against zebrafish IFT88 (1:5000), zebrafish IFT52 (1:5000), zebrafish IFT20 (1:5000), and zebrafish IFT57 (1:5000); and monoclonal anti–acetylated tubulin (1:10,000; Sigma).

## Results

We first examined *ift80* gene expression at multiple time points during development by in situ hybridization. Like other IFT genes, *ift80* was expressed maternally (data not shown). At 24 hpf, *ift80* was broadly expressed throughout the central nervous system (CNS) and the notochord (Fig. 1). CNS expression persisted through 72 hpf, though notochord expression diminished. Consistent with a role in cilia formation and function, *ift80* was expressed in the pronephric ducts (Fig. 1, arrow). We also observed expression in the pectoral fins, which are analogous to the mammalian limb bud. Noticeably, *ift80* expression was strongly expressed in the eye but not in the lens/cornea.

To test the function of *ift80*, we injected 1.5 ng morpholino oligonucleotide (MO) targeted to disrupt normal splicing of the *ift80* mRNA.[11] Morpholinos were targeted to the splice site at the 3′ end of the second exon (Fig. 2A) and were predicted to cause the loss of exon 3. Sequence analysis of cDNA from injected embryos revealed that 1.5 ng morpholino blocked the inclusion of exons 3 and 4 until at least 5 dpf (Fig. 2B; data not shown). To test whether the loss of *ift80* affected other components of the IFT particle, we examined extracts of whole embryos 5 dpf by Western blot analysis (Fig. 2D). The IFT particle consisted of two multi-subunit complexes, complex A (five proteins) and complex B (Ift80 and at least 10 other polypeptides).[37] Although not quantitative, Western blots of

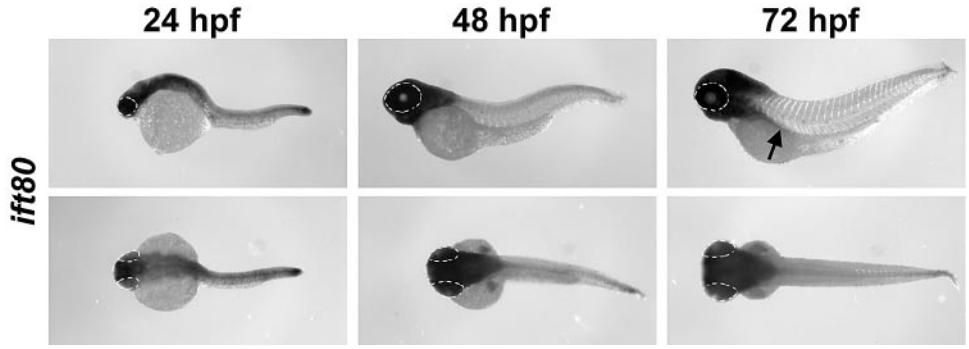


**FIGURE 1.** Expression of *ift80* during zebrafish development. Whole-mount in situ hybridization with an *ift80* riboprobe on 24 hpf, 48 hpf, and 72 hpf. *Top row*: lateral views. *Bottom row*: dorsal view. *Dashed lines*: eyes are outlined. *Arrow*: pronephric duct in the lateral view of the 72-hpf embryo.

protein extracts from *ift80* morphants appeared to contain similar amounts of the four other complex B proteins—Ift20, Ift52, Ift57, and Ift88. Because *ift80* is not predicted to be involved in transcriptional regulation, the qualitative increase of these proteins may reflect posttranslational stabilization. Interestingly, we previously found that loss of *ift57* in zebrafish reduced the level of complex B proteins.[32] It is unclear how different IFT components affect the stability of other IFT polypeptides.

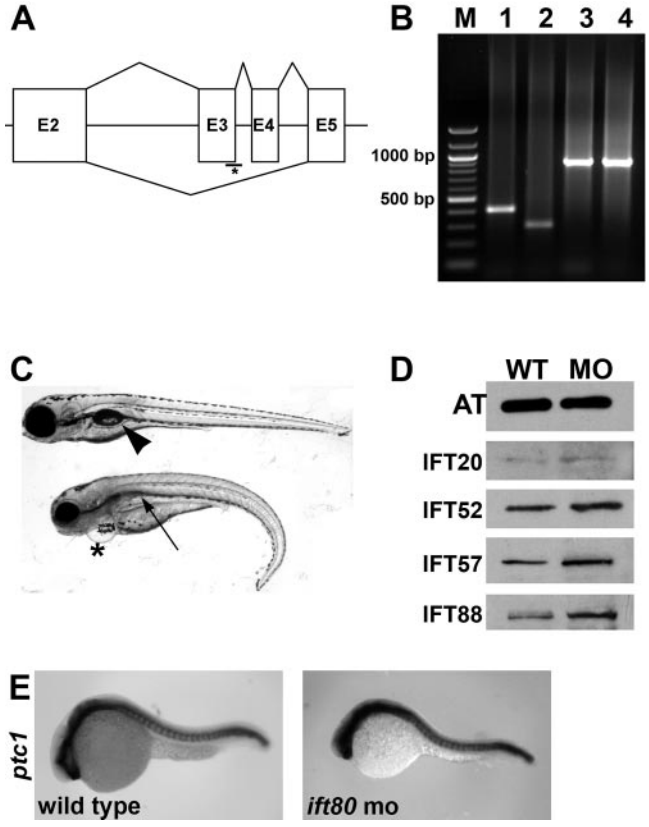


**FIGURE 2.** Loss of *ift80* function by morpholino knockdown. (**A**, *asterisk*) Diagram of splicing defect caused by the *ift80* morpholino targeted to the splice donor site on exon 3. After morpholino injection, both exons 3 and 4 are skipped (*bottom line*), resulting in a 180-bp deletion. (**B**) The DNA ladder marker (M) is shown at the far left. *Lane 1*, wild-type PCR product; *lane 2*, *ift80* morphant PCR product that is lower than the wild type product and consistent in size with loss of exons 3 and 4; *lanes 3* and *4*, β-actin PCR product from the wild-type and morphant cDNA samples, respectively, as a control. (**C**, *top*) 5-dpf wild-type control animal; (*bottom*) 5-dpf *ift80* morphant animal. *Asterisk*: heart edema in *ift80* morphant. Kidney cysts (*arrow*) are distinct from the swim bladder (*arrowhead*) seen in the wild-type animal. (**D**) Western blot analysis of IFT proteins from an *ift80* morphant. Protein extracts from 5-dpf wild-type and morphant animals were blotted with antibodies against IFT20, IFT52, IFT57, and IFT88. Acetylated tubulin (AT) was included as a loading control. (**E**) Whole-mount in situ hybridization of 24 hpf wild-type and *ift80* morphant with *ptc1* riboprobe.

Embryos injected with an *ift80*-MO had a ventral tail curvature, slightly smaller eyes, pericardial edema, and kidney cysts (Fig. 2C) at 5 dpf. The phenotype of MO-injected animals was similar to that of previously described IFT mutants[7,32] and consistent with defects in cilia function. Whole-mount immunostaining on embryos injected with *ift80*-MO with an antibody for acetylated tubulin revealed subtle defects of cilia in the ear and pronephric duct at 30 hpf (Supplementary Material, http://www.iovs.org/cgi/content/full/51/7/3792/DC1). Importantly, *ift80* morphants did not exhibit a noticeable optokinetic response under normal lighting conditions at 5 dpf (data not shown). IFT has been implicated in mammalian Hedgehog signaling,[22] and knockdown of *ift80* was previously reported to reduce the expression of *ptc1*, a downstream target of Hedgehog signaling.[11] As was shown, however, for previously described zebrafish IFT mutants,[38] *ptc1* expression was unchanged at 24 hpf after injection of *ift80* morpholino (Fig. 2E). One possible explanation for the difference between our result and the effects on Hedgehog signaling previously reported for this morpholino[11] is that we injected less morpholino to achieve full knockdown (1.5 ng vs. 4.0 ng). When injecting higher doses of morpholino, we observed necrosis in the brain and somites (data not shown).

Because *ift80* morphants did not exhibit visual function by optokinetic response assays, we performed histologic analysis to further examine the underlying visual defect. Retinal development proceeded normally in the absence of *ift80* function, but eye size and photoreceptor survival were disrupted (Fig. 3). At 60 hpf, wild-type animals exhibited optic nerves and distinct nuclear layers (Fig. 3A). For the next 2 to 3 days, the eye continued to grow, and photoreceptor outer segments became apparent, particularly in the ventral retina (Figs. 3B–D). At 60 hpf, *ift80* morphants displayed optic nerves and retinal lamination, as did wild-type embryos, though some disorganization was apparent (Fig. 3E). By 5 dpf, the eyes of *ift80*-MO–injected embryos were smaller than those wild-type controls, and very few outer segments were seen (Figs. 3F–H), similar to phenotypes observed in zebrafish IFT mutants.[7,32,39] Pyknotic nuclei and acellular holes were seen in all cellular layers in the *ift80*-MO retinas but were rarely observed in wild-type retinas (Figs. 3E, 3G, 3H; arrows). These results suggested that the small eye phenotype observed in *ift80*-MO–injected animals likely reflected the combination of cell death throughout the retinal and loss of volume normally occupied by photoreceptor outer segments. To test the hypothesis of cell death, TUNEL staining was performed on wild-type and *ift80* morphant retinas at 60 hpf, 72 hpf, 96 hpf, and 5 dpf, and the number of apoptotic nuclei was quantified (Fig. 4). In

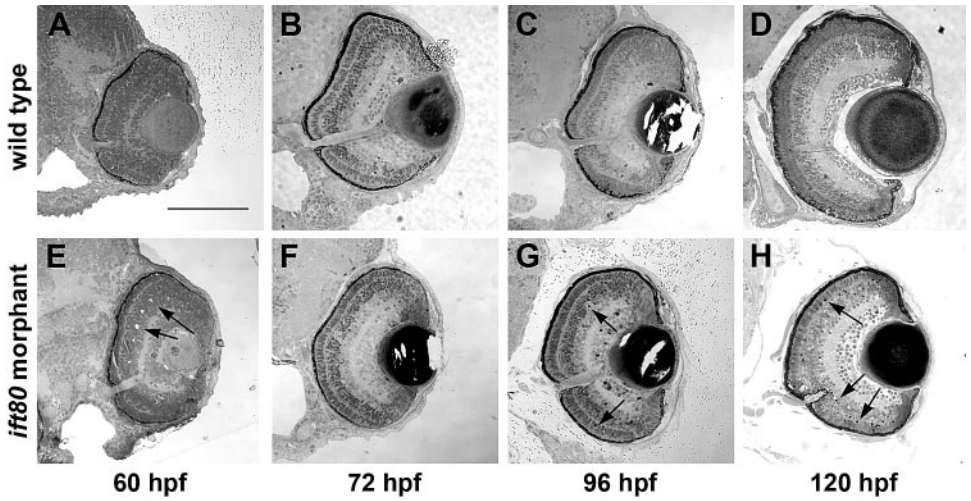


**FIGURE 3.** *ift80* morphants exhibit retinal degeneration. Transverse histologic sections through wild-type and *ift80* morphant retinas at several stages of development are shown. Wild-type zebrafish retina at (**A**) 60 hpf, (**B**) 72 hpf, (**C**) 96 hpf, and (**D**) 120 hpf. Retinas from *ift80* morphants at (**E**) 60 hpf, (**F**) 72 hpf, (**G**) 96 hpf, and (**H**) 120 hpf. *Arrows*: in *ift80* morphants, few outer segments are observed, and several pyknotic nuclei and acellular holes are seen. Scale bar, 100 $\mu$m.

wild-type animals, the number of TUNEL$^+$ cells was 1.3 ± 0.1 (mean ± SEM) at 60 hpf, 2.8 ± 0.4 at 72 hpf, 1.5 ± 0.2 at 96 hpf, and 0.4 ± 0.1 at 5 dpf. This is similar to a previous report showing cell death is highest at 72 hpf and declines by 5 dpf.[40] The total number of TUNEL$^+$ cells in *ift80* morphant retinas was not statistically different from that in controls at 60 hpf and 72 hpf (1.5 ± 0.2 and 3.8 ± 0.5, respectively), though considerable variation was observed in both wild-type and morphant analyses (Fig. 4B). The total number of TUNEL$^+$ cells was statistically higher in the *ift80* morphant retinas than in controls at both 96 hpf (2.6 ± 0.4 vs. 1.5 ± 0.2) and 5 dpf (7.4 ± 0.9 vs. 0.4 ± 0.1). Apoptosis within the photoreceptor layer of *ift80* morphants was elevated at 72 hpf, 96 hpf, and 5 dpf; most photoreceptors died at 5 dpf (Fig. 4C).

Disrupted photoreceptor outer segments were easily observed in *ift80*-MO animals by transmission electron microscopy. In control animals, rod and cone photoreceptor outer segments extended toward the retinal pigment epithelium at 5 dpf (Figs. 5A, 5B). In contrast, the few existing outer segments were shorter and highly disorganized after injection of *ift80*-MO (Figs. 5C–F). Cellular debris and pyknotic nuclei were seen in *ift80* morphants. Connecting cilia were seen in those *ift80* morphant photoreceptors with an outer segment but whose disc membranes were occasionally disordered. These results indicate that loss of *ift80* does not completely block outer segment formation but that *ift80* is necessary for proper organization of disc membranes and photoreceptor survival.

Given that outer segment assembly requires rhodopsin transport and defects in other IFT genes lead to rhodopsin mislocalization in zebrafish,[2,32] we hypothesized that the morphant photoreceptor phenotypes reflected defects in the transport of outer segment membrane proteins. A monoclonal antibody against rhodopsin, 1D1, labeled outer segments of wild-type zebrafish at 5 dpf (Fig. 6A). The *ift80* morphants exhibited

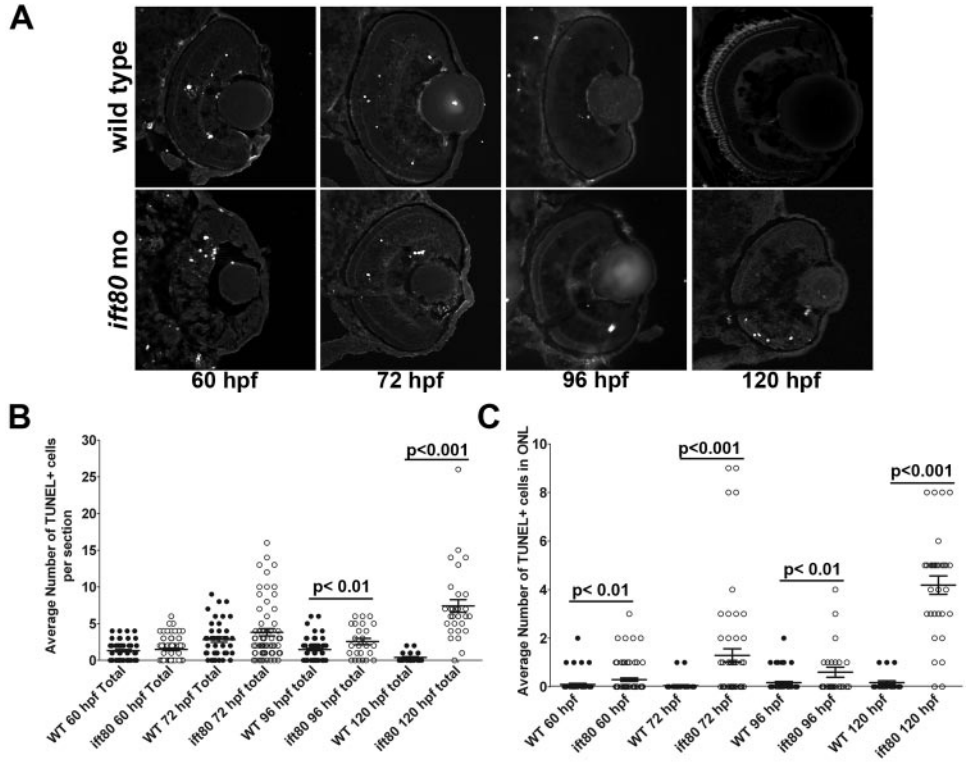


**FIGURE 4.** *ift80* morphants exhibited retinal degeneration. (**A**) TUNEL$^+$ cells were observed in wild-type and *ift80* morphants at 60 hpf, 72 hpf, 96 hpf, and 5 dpf. (**B**) Total number of TUNEL$^+$ cells and (**C**) number of TUNEL$^+$ cells in the outer nuclear layer (ONL) were quantified at each developmental stage for wild-type (*closed circles*) and *ift80* morphants (*open circles*), as shown in dot blots. Mean ± SEM for each time point is shown. Student's *t*-test was used to compare values for statistical significance.

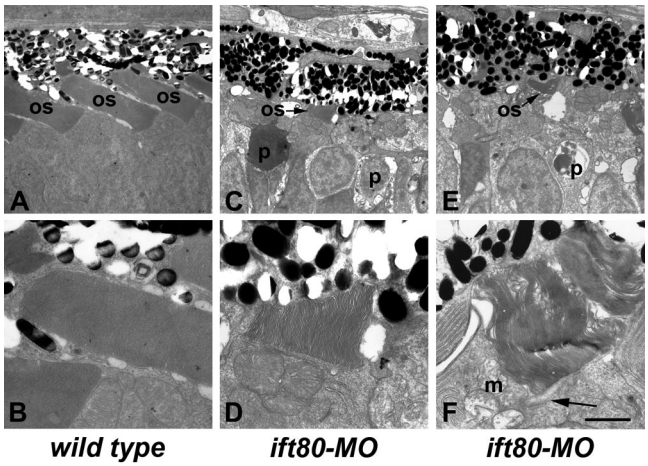


**FIGURE 5.** *ift80* morphants make cilia and disorganized outer segments. Transmission electron microscopy of 4-dpf wild-type and dynein morphant retinas are shown. (**A**) Wild-type photoreceptor outer segments (OS) are extending toward the RPE and are regularly spaced. (**B**) Higher-magnification image highlights the regular spacing of the disc membranes within the wild-type outer segments. (**C**–**F**) *ift80* morphants had very short outer segments (OS; *arrow*) and numerous pyknotic nuclei (p) in the photoreceptor layer. Disc membranes were disorganized, and mitochondria (m) were abnormal. (**F**, *arrow*) Connecting cilia were present. Scale bars: (**A**, **C**, **E**) 5 μm; (**B**, **D**, **F**) 2 μm.

significant mislocalization of rhodopsin, though some staining was observed in the outer segments (Fig. 6B). Blue opsin was expressed in the long single cones of zebrafish[41] and localized to the outer segment at 5 dpf (Fig. 6C). In contrast, injection of *ift80*-MO resulted in considerable mislocalization to the inner segment and a reduction in outer segment staining (Fig. 6D). Because opsin mislocalization can result in photoreceptor degeneration, cone morphology was examined using the zpr-1 antibody, which recognizes a cell-surface epitope on red-green double cones. Staining with zpr-1 showed wild-type cones with a tightly packed columnar morphology in the photoreceptor layer (Fig. 6E). The *ift80* morphants exhibited significant alterations in photoreceptor morphology indicative of degeneration and consistent with electron microscopy results (Fig. 6F).

We next examined whether components of the IFT machinery and axoneme were properly positioned. Centrin is a calcium-binding protein and a component of the basal body.[36] Centrin localized to the base of the connecting cilium of wild-type photoreceptors (Figs. 6G, 6H; arrows). Centrin immunoreactivity was also detected near the outer plexiform layer. We did not observe significant colocalization between centrin and acetylated tubulin in the cilium, which we attributed to the low signal from acetylated tubulin in the basal body region. Injection of *ift80*-MO did not eliminate centrin from the apical inner segment in most cells (Fig. 6H; arrows), but we did observe some centrin mislocalization throughout the inner segment (Fig. 6H; arrowheads) that was not observed in controls. IFT particle components Ift52 and Ift88 also localized to the connecting cilium of wild-type photoreceptors (Figs. 6I, 6K; arrows). Fewer connecting cilia were present in embryos after *ift80*-MO injection; however, both IFT52 and IFT88 remained colocalized with cilia (Figs. 6J, 6L; arrows). These results indicated that loss of *ift80* disrupts opsin trafficking to the outer segment and leads to photoreceptor degeneration but does not significantly affect the localization of proteins required for ciliogenesis.

JATD exhibits traits similar to those in BBS, and reduction of *BBS* gene function compromises Wnt/planar cell polarity

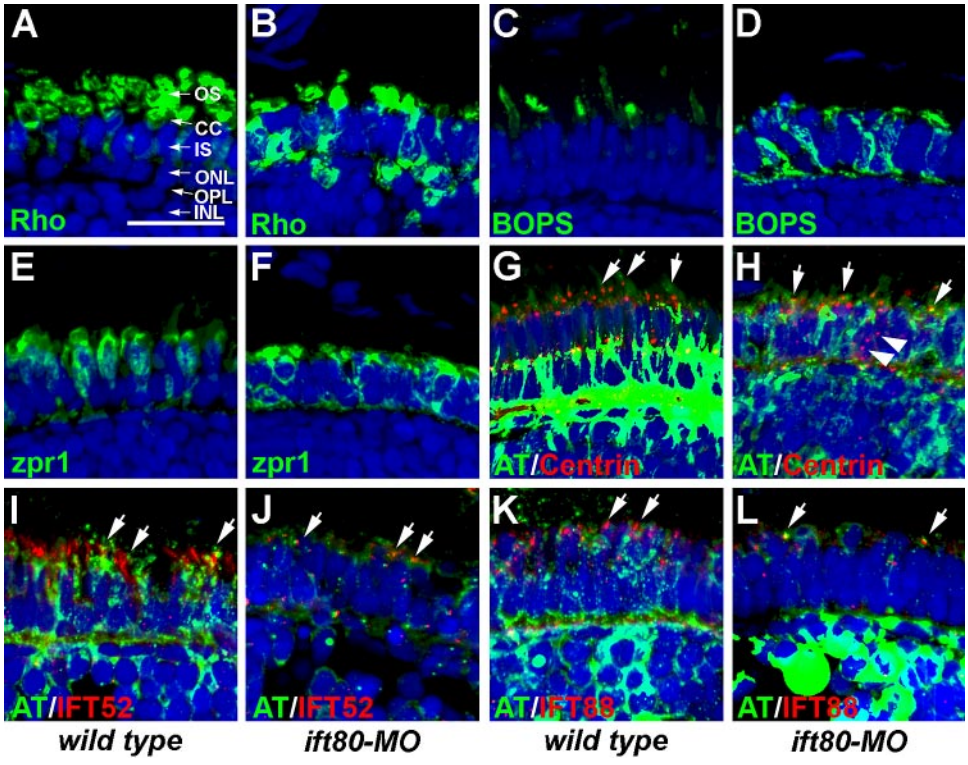


**FIGURE 6.** Immunohistochemical analysis of wild-type and *ift80* morphants at 5 dpf. (**A**) 1D1 (*green*), a marker for rhodopsin (Rho), localized to the outer segment region in wild-type fish. (**B**) Strong mislocalization to the inner segment was observed in *ift80* morphants. (**C**, **D**) Blue opsin (BOPS) was localized to the outer segments of wild-type photoreceptors. Strong mislocalization was seen in the *ift80* morphants. (**E**, **F**) Zpr1 (*green*), a label for red/green double cones, gave an elongated, columnar morphology in wild-type animals. Cone morphology was disheveled in the *ift80* morphants. (**G**, **H**) Centrin (*red*) localized to the apical surface of the inner segment (*short arrows*). Acetylated tubulin (AT; *green*) denotes microtubules labeled by anti–acetylated tubulin. Centrin was occasionally observed to be mislocalized (**H**; *white arrowheads*). (**I**, **J**) Ift52 (*red*) colocalized with acetylated tubulin (*green*) in the connecting cilia of wild-type and *ift80* morphants (*arrows*). (**K**, **L**) Ift88 (*red*) also showed strong apical localization in wild-type and *ift80* morphants. The number of Ift52- and Ift88-stained foci was significantly reduced in the *ift80* morphant retinas. Staining overlapped with AT (*green*). In all images, the tissues were counterstained with DAPI (*blue*). Outer segments (OS), connecting cilia (CC), inner segment (IS), outer nuclear layer (ONL), outer plexiform layer (OPL), and inner nuclear layer (INL) are shown for orientation purposes. Scale bar, 20 μm.

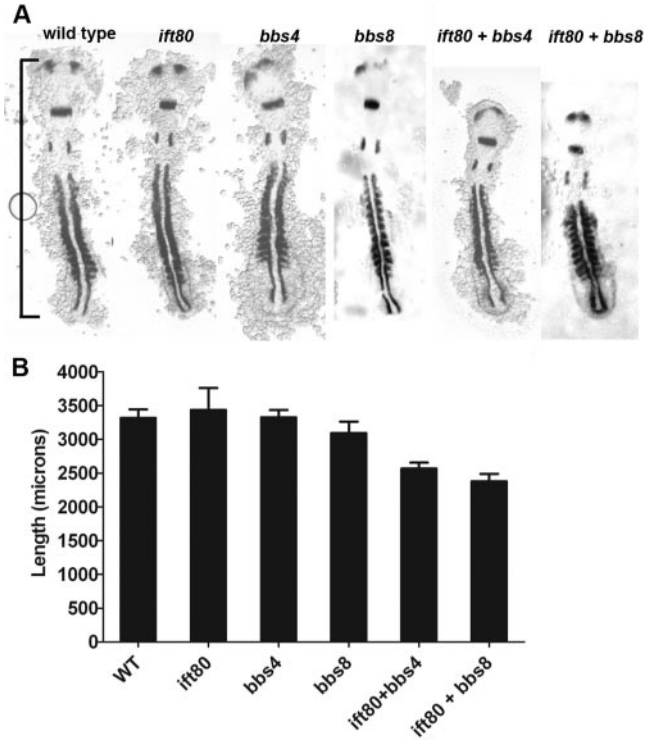


**FIGURE 7.** *ift80* interacts genetically with BBS genes. (**A**) Whole-mount in situ hybridization of embryos injected with 1.5 ng ift80 morpholino (*ift80*), 1.0 ng bbs8 morpholino (*bbs8*) or 1.0 ng bbs4 morpholino (*bbs4*), either alone or in combination. Embryos were fixed at the 10- to 12-somite stage and stained with *myoD* and *pax2a* riboprobes. All embryos were flat-mounted and photographed from the dorsal side, with the anterior portion at the *top*. (**B**) Body axis lengths were measured from the anteriormost region of *pax2a* staining to the tip of the paraxial mesoderm *myoD* staining (**A**, *bracket*). Bars represent the mean for each set of embryos ($n \geq 4$), and error bars are SEM. No statistical difference (*t*-test) from wild-type was found for any morpholino treatment alone. Injection of *ift80* morpholino in combination with either *bbs* morpholino decreased body length ($P < 0.005$).

(PCP) signaling in tissue culture and zebrafish embryos.[21,30,42] The basal body is proposed to serve as a key organelle for intracellular signaling,[43] and depletion of basal body proteins disrupts Wnt/PCP signaling during gastrulation. Injection of morpholinos targeted against zebrafish *bbs* genes leads to convergence-extension phenotypes, similar to those seen in the zebrafish mutants *trilobite* (the zebrafish *vangl2* ortholog) and *pipetail* (*wnt5*).[30] Given the similarity between JATD and BBS and given that basal body components were occasionally mislocalized in *ift80* morphant photoreceptors, we looked for genetic interactions between *ift80* and the *bbs* genes. In embryos injected with morpholinos against *ift80* (1.5 ng) or a modest dose of *bbs4* (1.0 ng) or *bbs8* (1.0 ng), the expression of *myoD* (somite) and *pax2a* (otic vesicle and forebrain) was similar to that of wild-type embryos at the 12- to 14-somite stage during gastrulation and early somitogenesis (Fig. 7A). However, embryos injected with a combination of morpholinos against *ift80* (1.5 ng) and *bbs4* (1.0 ng) or *ift80* and *bbs8* exhibited significant shortening of the body axis (Figs. 7A, 7B), indicating a synthetic genetic interaction between *ift80* and *bbs* genes.

## DISCUSSION

Zebrafish depleted of *ift80* exhibited photoreceptor degeneration and surviving photoreceptors had shortened outer segments with mislocalized rod and cone opsin proteins. Given the importance of IFT in cilia biogenesis and maintenance, it was not surprising that loss of *ift80* resulted in phenotypes similar to those reported for other zebrafish IFT mutants or morphants.[7,32,44] Although photoreceptors degenerated in the *ift80* morphants, outer segment formation was not blocked, implying that *ift80* is required for outer segment maintenance but not for ciliogenesis. Thus, the vision loss described in some patients with JADT likely reflects photoreceptor degeneration rather than a morphogenesis failure or a nonphotoreceptor defect. Although vision loss has been described in some patients with JATD,[14,15] the three alleles of *IFT80* that cause JATD were not present in renal or retinal phenotypes.[11] In that study, two alleles were missense mutations, and one was an in-frame deletion. These mutations may be hypomorphic, or, in distinct domains of the Ift80 protein, they may result in retinal degeneration. Future identification and analysis of *IFT80* alleles in patients with JATD and vision loss will help explain the range of phenotypes observed by *IFT80* mutation.

Previous studies of *ift80* in invertebrate systems suggested a role in the biogenesis of cilia more pronounced than that seen in zebrafish. Knockdown of *Ift80* in *Tetrahymena* abolished cilia formation,[11] whereas nonsense alleles of *ift80* (*che-2*) in *Caenorhabditis elegans* resulted in very short cilia in sensory neurons.[45] Nevertheless, the *ift80/che-2* mutant phenotype reflected ciliogenesis failure rather than cilia degeneration.[45] Although ciliogenesis occurs in zebrafish *ift80* morphants, it is unlikely that photoreceptors and other cilia complete normal morphogenesis before degeneration. No examples of such phenomena have been reported for null IFT mutants. Mutations in *ift80* have not been described in *Chlamydomonas* or mouse, and no direct binding partners are known. It is unclear why loss of *ift80* does not completely abolish ciliogenesis and block outer segment formation in zebrafish, but the trafficking phenotypes we observed indicated the IFT particle remained sufficiently intact to bind some ciliary cargo and underwent limited IFT. Although several *Chlamydomonas* IFT mutants show destabilization of the IFT particles and reductions in IFT proteins, our results show that components of the IFT complex B are more abundant in *ift80* morphant zebrafish. As a component of IFT complex B, the Ift80 protein readily dissociated from the core complex under high salt conditions, suggesting Ift80 may reside on the surface of complex B.[46] The Ift57 protein also dissociated from complex B under high salt conditions, and mutation of *ift57* in zebrafish resulted in short outer segments, similar to those seen in *ift80* morphants.[32] Thus, though loss of Ift80 may not dramatically destabilize the remaining particle, it clearly disrupts overall IFT function.

We show that *ift80* genetically interacts and produces synthetic phenotypes with *bbs* genes. BBS proteins are components of the basal body that also mediate cilia biogenesis.[47,48] Recent studies suggest the cilia and basal body are distinct organelles and the basal body mediates Wnt signaling, as evidenced by genetic interactions between *bbs* genes and the noncanonical Wnt pathway, also known as the PCP pathway.[30] We show that morpholino knockdown of *ift80* with *bbs4* or *bbs8* reduced the body axis and led to mild convergence-extension defects, a phenotype associated with defective Wnt/PCP signaling. Given that proper cell polarity and basal body positioning are essential for photoreceptor morphogenesis, it is intriguing to consider a role for Wnt/PCP signaling in outer segment formation. The role of IFT proteins in Wnt/PCP signaling, however, is controversial.[49–51] Null alleles of several mouse and zebrafish IFT genes show no defects in Wnt signal-

ing during gastrulation.[50,51] However, a conditional knockout allele of *Ift88* can disrupt cell polarity within the inner ear, as can mutations in *Bbs6* and *Bbs4*.[42,49] Perhaps *ift80* has dual roles in IFT and basal body function. It is interesting that zebrafish *bbs* genes showed genetic interactions with *ift80*. When analyzing IFT movement in sensory neurons of *C. elegans*, mutation of *BBS8* had little effect on the movement of *Ift80* protein, suggesting there was no direct contact, whereas mutation of either *BBS7* or *BBS8* severely compromised the movement of OSM-5/Ift88.[52] Future research will be necessary to determine whether the BBS proteins directly interact with Ift80 in zebrafish and whether such interactions regulate distinct functions in ciliary transport and photoreceptor cell polarity.

## *References*


1. Satir P, Christensen ST. Overview of structure and function of mammalian cilia. *Annu Rev Physiol.* 2007;69:377–400.
2. Insinna C, Besharse JC. Intraflagellar transport and the sensory outer segment of vertebrate photoreceptors. *Dev Dyn.* 2008;237:1982–1992.
3. Badano JL, Mitsuma N, Beales PL, Katsanis N. The ciliopathies: an emerging class of human genetic disorders. *Annu Rev Genomics Hum Genet.* 2006;7:125–148.
4. Adams NA, Awadein A, Toma HS. The retinal ciliopathies. *Ophthalmic Genet.* 2007;28:113–125.
5. Rosenbaum J. Intraflagellar transport. *Curr Biol.* 2002;12:R125.
6. Pazour GJ, Baker SA, Deane JA, et al. The intraflagellar transport protein, IFT88, is essential for vertebrate photoreceptor assembly and maintenance. *J Cell Biol.* 2002;157:103–113.
7. Tsujikawa M, Malicki J. Intraflagellar transport genes are essential for differentiation and survival of vertebrate sensory neurons. *Neuron.* 2004;42:703–716.
8. Sukumaran S, Perkins BD. Early defects in photoreceptor outer segment morphogenesis in zebrafish ift57, ift88 and ift172 intraflagellar transport mutants. *Vision Res.* 2009;49:479–489.
9. Jeune M, Beraud C, Carron R. Asphyxiating thoracic dystrophy with familial characteristics. *Arch Fr Pediatr.* 1955;12:886–891.
10. Jeune M, Carron R, Beraud C, Loaec Y. Polychondrodystrophie avec blocage thoracique d'evolution fatale. *Pediatrie.* 1954;9:390–392.
11. Beales PL, Bland E, Tobin JL, et al. IFT80, which encodes a conserved intraflagellar transport protein, is mutated in Jeune asphyxiating thoracic dystrophy. *Nat Genet.* 2007;39:727–729.
12. Oberklaid F, Danks DM, Mayne V, Campbell P. Asphyxiating thoracic dysplasia: clinical, radiological, and pathological information on 10 patients. *Arch Dis Child.* 1977;52:758–765.
13. Johnson CA, Gissen P, Sergi C. Molecular pathology and genetics of congenital hepatorenal fibrocystic syndromes. *J Med Genet.* 2003;40:311–319.
14. Casteels I, Demandt E, Legius E. Visual loss as the presenting sign of Jeune syndrome. *Eur J Paediatr Neurol.* 2000;4:243–247.
15. Phillips CI, Stokoe NL, Bartholomew RS. Asphyxiating thoracic dystrophy (Jeune's disease) with retinal aplasia: a sibship of two. *J Pediatr Ophthalmol Strabismus.* 1979;16:279–283.
16. Bard LA, Bard PA, Owens GW, Hall BD. Retinal involvement in thoracic-pelvic-phalangeal dystrophy. *Arch Ophthalmol.* 1978;96:278–281.
17. Allen AW Jr, Moon JB, Hovland KR, Minckler DS. Ocular findings in thoracic-pelvic-phalangeal dystrophy. *Arch Ophthalmol.* 1979;97:489–492.
18. Wilson DJ, Weleber RG, Beals RK. Retinal dystrophy in Jeune's syndrome. *Arch Ophthalmol.* 1987;105:651–657.
19. Leitch CC, Zaghloul NA, Davis EE, et al. Hypomorphic mutations in syndromic encephalocele genes are associated with Bardet-Biedl syndrome. *Nat Genet.* 2008;40:443–448.
20. Badano JL, Leitch CC, Ansley SJ, et al. Dissection of epistasis in oligogenic Bardet-Biedl syndrome. *Nature.* 2006;439:326–330.
21. Khanna H, Davis EE, Murga-Zamalloa CA, et al. A common allele in RPGRIP1L is a modifier of retinal degeneration in ciliopathies. *Nat Genet.* 2009;41:739–745.
22. Huangfu D, Anderson KV. Cilia and Hedgehog responsiveness in the mouse. *Proc Natl Acad Sci U S A.* 2005;102:11325–11330.
23. Huangfu D, Liu A, Rakeman AS, Murcia NS, Niswander L, Anderson KV. Hedgehog signalling in the mouse requires intraflagellar transport proteins. *Nature.* 2003;426:83–87.
24. Houde C, Dickinson RJ, Houtzager VM, et al. Hippi is essential for node cilia assembly and Sonic hedgehog signaling. *Dev Biol.* 2006;300:523–533.
25. Liu A, Wang B, Niswander LA. Mouse intraflagellar transport proteins regulate both the activator and repressor functions of Gli transcription factors. *Development.* 2005;132:3103–3111.
26. Brockerhoff SE, Hurley JB, Janssen-Bienhold U, Neuhauss SC, Driever W, Dowling JE. A behavioral screen for isolating zebrafish mutants with visual system defects. *Proc Natl Acad Sci U S A.* 1995;92:10545–10549.
27. Schmitt EA, Dowling JE. Early retinal development in the zebrafish, *Danio rerio*: light and electron microscopic analyses. *J Comp Neurol.* 1999;404:515–536.
28. Westerfield M. *The Zebrafish Book*. 3rd ed. Eugene, OR: University of Oregon Press; 1995.
29. Detrich HW III, Zon LI, Westerfield M. *Methods in Cell Biology*. 2nd ed. New York: Academic Press; 2004.
30. Gerdes JM, Liu Y, Zaghloul NA, et al. Disruption of the basal body compromises proteosomal function and perturbs intracellular Wnt response. *Nat Genet.* 2007;39:1350–1360.
31. Yen HJ, Tayeh MK, Mullins RF, Stone EM, Sheffield VC, Slusarski DC. Bardet-Biedl syndrome genes are important in retrograde intracellular trafficking and Kupffer's vesicle cilia function. *Hum Mol Genet.* 2006;15:667–677.
32. Krock BL, Perkins BD. The intraflagellar transport protein IFT57 is required for cilia maintenance and regulates IFT-particle-kinesin-II dissociation in vertebrate photoreceptors. *J Cell Sci.* 2008;121:1907–1915.
33. Jowett T, Lettice L. Whole-mount in situ hybridizations on zebrafish embryos using a mixture of digoxigenin- and fluorescein-labelled probes. *Trends Genet.* 1994;10:73–74.
34. Perkins BD, Nicholas CS, Baye LM, Link BA, Dowling JE. dazed gene is necessary for late cell type development and retinal cell maintenance in the zebrafish retina. *Dev Dyn.* 2005;233:680–694.
35. Vihtelic TS, Doro CJ, Hyde DR. Cloning and characterization of six zebrafish photoreceptor opsin cDNAs and immunolocalization of their corresponding proteins. *Vis Neurosci.* 1999;16:571–585.
36. Giessl A, Pulvermuller A, Trojan P, et al. Differential expression and interaction with the visual G-protein transducin of centrin isoforms in mammalian photoreceptor cells. *J Biol Chem.* 2004;279:51472–51481.
37. Rosenbaum JL, Witman GB. Intraflagellar transport. *Nat Rev Mol Cell Biol.* 2002;3:813–825.
38. Lunt S, Haynes T, Perkins BD. Zebrafish ift57, ift88, and ift172 intraflagellar transport mutants disrupt cilia but do not affect Hedgehog signaling. *Dev Dyn.* 2009;238:1744–1759.
39. Gross JM, Perkins BD, Amsterdam A, et al. Identification of zebrafish insertional mutants with defects in visual system development and function. *Genetics.* 2005;170:245–261.
40. Biehlmaier O, Neuhauss SC, Kohler K. Onset and time course of apoptosis in the developing zebrafish retina. *Cell Tissue Res.* 2001;306:199–207.
41. Raymond PA, Barthel LK, Rounsifer ME, Sullivan SA, Knight JK. Expression of rod and cone visual pigments in goldfish and zebrafish: a rhodopsin-like gene is expressed in cones. *Neuron.* 1993;10:1161–1174.
42. Ross AJ, May-Simera H, Eichers ER, et al. Disruption of Bardet-Biedl syndrome ciliary proteins perturbs planar cell polarity in vertebrates. *Nat Genet.* 2005;37:1135–1140.
43. Berbari NF, O'Connor AK, Haycraft CJ, Yoder BK. The primary cilium as a complex signaling center. *Curr Biol.* 2009;19:R526–R535.
44. Krock B, Mills-Henry I, Perkins B. Retrograde intraflagellar transport by cytoplasmic dynein-2 is required for outer segment exten-

sion in vertebrate photoreceptors but not arrestin translocation. *Invest Ophthalmol Vis Sci.* 2009;50:5463–5471.

45. Fujiwara M, Ishihara T, Katsura I. A novel WD40 protein, CHE-2, acts cell-autonomously in the formation of C. elegans sensory cilia. *Development.* 1999;126:4839–4848.
46. Lucker BF, Behal RH, Qin H, et al. Characterization of the intraflagellar transport complex B core: direct interaction of the IFT81 and IFT74/72 subunits. *J Biol Chem.* 2005;280:27688–27696.
47. Ansley SJ, Badano JL, Blacque OE, et al. Basal body dysfunction is a likely cause of pleiotropic Bardet-Biedl syndrome. *Nature.* 2003; 425:628–633.
48. Nachury MV, Loktev AV, Zhang Q, et al. A core complex of BBS proteins cooperates with the GTPase Rab8 to promote ciliary membrane biogenesis. *Cell.* 2007;129:1201–1213.
49. Jones C, Roper VC, Foucher I, et al. Ciliary proteins link basal body polarization to planar cell polarity regulation. *Nat Genet.* 2008;40:69–77.
50. Huang P, Schier AF. Dampened Hedgehog signaling but normal Wnt signaling in zebrafish without cilia. *Development.* 2009;136: 3089–3098.
51. Ocbina PJ, Anderson KV. Intraflagellar transport, cilia, and mammalian Hedgehog signaling: analysis in mouse embryonic fibroblasts. *Dev Dyn.* 2008;237:2030–2038.
52. Blacque OE, Reardon MJ, Li C, et al. Loss of *C. elegans* BBS-7 and BBS-8 protein function results in cilia defects and compromised intraflagellar transport. *Genes Dev.* 2004;18:1630–1642.
53. Kramer-Zucker AG, Olale F, Haycraft CJ, Yoder BK, Schier AF, Drummond IA. Cilia-driven fluid flow in the zebrafish pronephros, brain and Kupffer's vesicle is required for normal organogenesis. *Development.* 2005;132:1907–1921.
54. Riley BB, Zhu C, Janetopoulos C, Aufderheide KJ. A critical period of ear development controlled by distinct populations of ciliated cells in the zebrafish. *Dev Biol.* 1997;191:191–201.